Fusion studies in $^{12}C + ^{182,184,186}W$ reactions at energies below and near the Coulomb barrier

S. Sanila,* A. M. Vinodkumar,† and B. R. S. Babu
Department of Physics, University of Calicut, Kerala 673635, India

N. Madhavan, S. Nath, J. Gehlot, Rohan Biswas, Chandra Kumar, and Gonika
Nuclear Physics Group, Inter University Accelerator Centre, New Delhi 110067, India

Anjali Rani, A. Parihari, and Dinesh Viswakarma
Department of Physics and Astrophysics, University of Delhi, Delhi 110007, India

Shoaib Noor
Department of Physics, Thapar University, Patiala 147004, India

E. Prasad
Department of Physics, School of Physical Sciences, Central University of Kerala, The Aswini Hills, Periya 671320, India

(Received 30 April 2022; accepted 26 July 2022; published 23 August 2022)

Background: The coupled-channels model has been highly successful in interpreting experimental subbarrier fusion. The statistical model framework has traditionally been used to explain the basic features of composite system de-excitation in the above Coulomb barrier region. However, in ^{12}C-induced reactions with $^{182,186}W$, measured fusion cross sections are significantly lower than those predicted by various theoretical models and by fusion systematics.
Purpose: To investigate the dynamics of heavy ion fusion at energies below and above the Coulomb barrier in the ^{12}C-induced reactions.
Method: A mass spectrometer was used to study the evaporation residues for the $^{12}C + ^{182,184,186}W$ reactions. The measurements ranged from 12% below to 45% above the Coulomb barrier energies. The measured fusion cross sections are compared with coupled channels and statistical model calculations.
Results: The measured fusion cross sections for $^{12}C + ^{182,184,186}W$ reactions show reasonably good agreement with coupled-channel calculations. Also, evaporation residue cross sections for $^{12}C + ^{182,184,186}W$ reactions in the present experiment along with the fission cross sections from literature are described by statistical model calculations.
Conclusions: We successfully explain the previously reported discrepancy between fusion measurements and calculations based on various theoretical models and by fusion systematics for $^{12}C + ^{182,186}W$ reactions.

DOI: 10.1103/PhysRevC.106.024614

I. INTRODUCTION

Heavy ion fusion studies can provide important insights into the reaction dynamics and decay properties of excited compound nuclei (CN) [1–11]. Nucleons are exchanged between the target and projectile during the mechanism of compound nucleus formation. As a result, energy and angular momentum are transferred from the relative motion to the intrinsic degrees of freedom of the composite system [12]. The formed compound nucleus is in a highly excited state and decays via the emission of light particles and γ-rays with competition from binary fission processes. Evaporation residue (ER) measurement is a powerful method for studying fusion processes in mass asymmetric projectile-target systems. Fission fragments must be taken into account when calculating total fusion cross sections and understanding the dynamics of the CN de-excitation. The statistical model framework has typically been used to explain the de-excitation of the composite system with the inclusion of fission processes. Even though the fundamental concepts of composite system de-excitation are relatively well understood by statistical model calculations, some discrepancies and/or ambiguities remain [13–15].

It is well known that the one-dimensional potential barrier penetration model (1D-BPM) is quite successful in reproducing the measured fusion cross sections at above barrier energies. The increase in subbarrier fusion cross sections in comparison to 1D-BPM is well explained by coupled-channel calculations, which include the coupling of low-lying states and the static deformation and/or vibrational degrees of

*sanila_dop@uoc.ac.in
†amv@uoc.ac.in

freedom of participating nuclei [16–20]. Beckerman *et al.* [21] reported the effects of the positive Q value of neutron transfer (PQNT) on the subbarrier fusion enhancement in ^{58}Ni + ^{64}Ni reaction for the the first time. Moreover, the influence of neutron transfer channels with positive Q values in fusion enhancement has been investigated by many researchers [2,22–30].

The experimental observation of an asymmetric fission in the ^{180}Hg [31] led to intensive theoretical and experimental studies of fission of Hg [32–45]. Andreev *et al.* [38] calculated the mass distributions for fission of different Hg isotopes using the improved scission-point models and compared the results with the experimental data [46]. They found that the mass distribution is quite asymmetric for ^{180}Hg and ^{184}Hg. For ^{188}Hg the asymmetry is less pronounced. In the case of ^{192,196}Hg and ^{198}Hg, the mass distribution looks more symmetric but with a dip on the top. Prasad *et al.* [34] observed mass asymmetric fission in neutron-deficient ^{182}Hg nuclei populated by heavy ion fusion. They suggested that the observed asymmetric fission in ^{182}Hg and its absence in ^{195}Hg is due to the difference in the dynamical evolution of ^{182}Hg and ^{195}Hg CN. Hg nuclei exhibit structural changes as one goes from neutron-deficient ^{180}Hg to relatively neutron-rich ^{198}Hg nuclei. Also, the asymmetric component in the mass distribution of fragments may be associated with quasifission (QF) [47–49]. This will have an effect on fission, fusion, and ER cross sections. Accordingly our fusion measurements are expected to throw light on the role of asymmetric component of mass distribution of fragments associated with QF.

Kozulin *et al.* [32] studied the dependence of the symmetric and asymmetric fission of ^{180,182,183}Hg and ^{178}Pt nuclei as a function of excitation energy and isospin. They found that the existence of well-deformed proton shell at $Z \approx 36$ and less deformed proton shell at $Z \approx 46$ as responsible for the new type of asymmetric fission in pre-actinide nuclei. Bogachev *et al.* [33] reported their findings on the asymmetric and symmetric fission modes in ^{180,190}Hg formed in the ^{36}Ar + ^{144,154}Sm reactions. They observed that proton numbers play a stabilizing role in the asymmetric fission of excited pre-actinide nuclei. Also, they found that the yield of symmetric fission for ^{190}Hg is lower than for ^{180}Hg at the same excitation energies of CN at the saddle point. Kozulin *et al.* [50] observed a large contribution (more than 70%) of QF in the case of ^{68}Zn + ^{112}Sn reaction. However, QF was not observed in the case of ^{36}Ar + ^{144}Sm reaction forming the same CN [35,45,47]. du Rietz *et al.* [51] analyzed a large set of experimental mass-angular distributions of fission-like fragments and found that the threshold value for the QF appearance for composite systems with $Z_{\rm CN} = 80$ is $Z_P Z_T = 1450 \pm 100$ (where $Z_{\rm CN}$, Z_P, and Z_T are the atomic number of the CN, projectile, and target respectively). Also, they reported that QF appears for the reactions with mean fissility parameter $\chi_m > 0.68$ and QF becomes dominant at $\chi_m > 0.765$. In the case of ^{68}Zn + ^{112}Sn, the value of χ_m (0.695) and the $Z_P Z_T$ (1500) are close to the threshold values for the onset of the QF processes. So such a large contribution of QF was unexpected. Kaur *et al.* [52] measured ER cross sections for ^{48}Ti + ^{140,142}Ce reactions forming ^{188,190}Hg CN to understand the influence of neutron shell closure of target nuclei on CN formation. They observed that the effects of shell closure in the target nucleus on fusion cross sections is negligible. Further, they found no evidence of QF processes in the ^{48}Ti + ^{140,142}Ce systems.

The fission cross sections for the systems ^{12}C + $^{182-186}$W were measured by many researchers [53–56]. Rajagopalan *et al.* [53] measured evaporation residues (ER), fission fragments (FF), and charged particle emission for the systems ^{12}C + ^{182}W, ^{19}F + ^{175}Lu, ^{20}Ne + ^{174}Yb, and ^{40}Ar + ^{154}Sm, forming ^{194}Hg at excitation energies ranging from 57 to 195 MeV. In the case of ^{12}C + ^{182}W reaction, their systematics-based calculations overestimate as compared to the measured fusion cross sections. However, measurements with heavier projectiles, ^{19}F, ^{20}Ne, and ^{40}Ar, all show reasonable agreement with the calculated cross sections. This discrepancy in the case of ^{12}C + ^{182}W is attributed to missing ER events due to small recoil energies in their detection system. Furthermore, Rajagopalan *et al.* have shown that nonequilibrium mechanisms have a bigger role in the ER cross sections in the case of ^{12}C and ^{19}F in comparison to ^{40}Ar-induced reactions.

Delagrange *et al.* [54] used a time-of-flight setup to measure the ER events in ^{12}C + ^{181}Ta and ^{12}C + ^{182,186}W reactions to investigate the inconsistency between measurements and calculations. Their measurements observed similar cross sections as Rajagopalan *et al.* [53] and attributed the discrepancies with calculations as due to the loss of ER events [54]. Furthermore, Delagrange *et al.* also measured fission cross sections for ^{12}C + ^{182,186}W reactions in the 56 to 87 MeV excitation energies. They observed a significant difference in the fission yield of ^{194}Hg CN in comparison to ^{198}Hg compound nuclei at $E^* = 82$ MeV ($\sigma_{\rm fiss} = 536 \pm 52$ mb for ^{194}Hg and $\sigma_{\rm fiss} = 166 \pm 68$ mb for ^{198}Hg). One of the explanations given for this discrepancy is that it is caused by the competition between evaporation of neutrons and fission. Stokstad *et al.* [14] reported lower values of the fusion cross sections for ^{40}Ar + ^{144,148}Sm at higher excitation energies compared to ^{40}Ar + ^{154}Sm, which formed ^{184,188,194}Hg respectively. They suggested that the lowering of the cross sections for ^{40}Ar + ^{144,148}Sm could be a result of the dynamic effects such as rotation of the target nuclei before fusion or the distortion of the target nucleus in the Coulomb field of the projectile.

Miller *et al.* [57] reported that the probability of ^{1}H and ^{4}He evaporation from ^{194}Hg CN increases rapidly with energy and appears to protect the system from fission. Rajagopalan *et al.* [53] confirmed that most ^{1}H and ^{4}He are evaporated prior to fission. Alexander *et al.* [58] have unfolded the effects of excitation energy and spin on the decay of ^{194}Hg CN. They suggested that at higher excitation energies ($E^* > 98$ MeV), the competition between fission and evaporation is highly sensitive to the relative values of the level densities. In order to study the spin dependence of dissipation effects in fission, Hui *et al.* [59] measured ER excitation function in coincidence with γ-ray multiplicity for the ^{19}F + ^{175}Lu reaction, forming ^{194}Hg CN. Their measurements show that there are no dissipation effects in the presaddle region of the fission processes.

Calculated fusion cross sections based on various theoretical models and systematics showed large deviation with respect to measured cross sections for ^{12}C + ^{182,186}W

reactions [53,54] in the laboratory energy range 77 to 167 MeV. However, fusion cross-section measurements with heavier projectiles forming ^{194}Hg CN follow the fusion systematics [53]. This necessitated measuring the ER cross sections for $^{12}C + ^{182,184,186}W$ forming ^{194,196,198}Hg nuclei. In the present work, we report the measurements of fusion-evaporation cross sections for $^{12}C + ^{182,184,186}W$ reactions at below and near Coulomb barrier energies.

This article is structured as follows. Section II discusses the experimental setup and procedure, Sec. III describes the analysis in detail, and Sec. IV discusses the details of the coupled channel and statistical model calculations, their comparison with the experimental cross sections, and their potential implications. Section V summarizes and concludes the work reported here.

II. EXPERIMENTAL DETAILS

The experiments were conducted at the Inter-University Accelerator Centre (IUAC) in New Delhi, using a ^{12}C beam with energies ranging from 52 to 84 MeV provided by the 15UD Pelletron Accelerator. We have used pulsed beam of ^{12}C with pulse separation 8 μs at 52–58 MeV, 4 μs at 60–72 MeV, and 500 ns at 76–84 MeV. The targets used were ^{182,184,186}W with thicknesses 70, 100, and 100 μg/cm^2 with carbon backing of 20, 35, and 25 μg/cm^2 respectively. The levels of enrichment for the ^{182,184,186}W targets were 91.6, 95.2, and 94.0% respectively.

Two silicon surface barrier detectors (monitors) were placed in the target chamber, one on each side of the beam direction, to measure the elastically scattered beam particles for normalization and absolute cross-section determination. These detectors, each with an active area of 50 mm^2 with a collimator diameter of 1 mm were placed ≈100 mm from the target at ±15° relative to the beam axis. A carbon charge reset foil with a large surface area and a thickness of ≈ 10 μg/cm^2 was placed 10 cm downstream of the target to reset the charge state of ERs. The Heavy Ion Reaction Analyzer (HIRA) [60] separated ERs from the beamlike background and transported them to its focal plane (FP). HIRA is set for the most dominant channel (HIRA has energy acceptance ±20% and mass acceptance ±5%). For these experiments, the solid angle of acceptance for HIRA was kept at 5 msr. A two-dimensional position-sensitive multiwire proportional counter (MWPC) with an active area of 15 × 5 cm was used at the HIRA's focal plane to detect ERs [61]. To separate the ERs from the beamlike particles, a time of flight (TOF) was set up between the anode of the MWPC and the RF signal of the beam pulsing system.

III. DATA ANALYSIS

Timing and energy-loss signals from the MWPC at the FP of the spectrometer, along with the position data obtained from the wire grids using a delay line technique, were processed using a Computer Automated Measurement And Control (CAMAC)-based data acquisition system. The data is analyzed in offline mode using the software CANDLE [62]. The coincidence spectrum between energy loss, ΔE (from the MWPC cathode), and TOF was used to extract ER yields. The experimental data were normalized by dividing the ER counts (Y_{ER}) by the elastic scattering counts in the forward-angle normalization detectors (Y_{nom}). We calculated the transmission efficiency (ϵ_{HIRA}) of the HIRA using the Monte Carlo code TERS [63]. The total ER cross section was extracted using Eq. (1),

$$\sigma_{ER} = \frac{Y_{ER}}{Y_{nom}} \left(\frac{d\sigma}{d\Omega}\right)_{Ruth} \Omega_{nom} \frac{1}{\epsilon_{HIRA}} \tag{1}$$

where $(\frac{d\sigma}{d\Omega})_{Ruth}$ is the differential Rutherford-scattering cross sections in the laboratory system.

The transmission efficiency of the recoil mass separator, HIRA, is one of the most important factors in any experiment. Relative populations of all possible ER channels have been estimated using statistical model code PACE4 [64,65]. Based on these relative populations, the efficiency of HIRA is calculated for all evaporation channels that account for more than 1% of total fusion cross sections. The transmission efficiency at any given energy is calculated by taking the weighted average of each individual channel efficiencies. The estimated error in HIRA efficiency is ≈10% for $^{12}C + ^{182,184,186}W$ reactions. In Table I, we have listed the measured ER cross sections for the $^{12}C + ^{182,184,186}W$ reactions as a function of energy. The quoted errors in Table I include the statistical error plus the error in the estimation of transmission efficiency.

IV. RESULTS AND DISCUSSION

A simple one-dimensional barrier penetration model (1D-BPM) fails to explain the observed subbarrier cross sections [1]. The basic features of nuclear reactions in 1D-BPM are commonly described in terms of interaction that is expressed solely as a function of nuclear radial separation. The formation of the CN at energies near and below the Coulomb barrier is strongly influenced by coupling between deformation or orientation and nuclear intrinsic motions of the colliding nuclei. The coupled-channels (CC) approach includes such channel coupling effects in the potential barrier and replaces a single barrier with a distribution of barriers [1]. Tunneling through a multidimensional potential barrier successfully explains the observed experimental subbarrier fusion enhancement [1,2,66]. The present measurements were analyzed using coupled-channel calculations to investigate the effects of coupling of different excited states of the target nuclei in the subbarrier energy region. The CN is a very complex many-body system, and its decay is typically handled by statistical evaporation models, so we used statistical model calculations to estimate ER cross sections for $^{12}C + ^{182,184,186}W$ reactions and to study the fission-evaporation competition of the Hg CN.

A. Coupled-channel calculations

The coupled-channel code CCFULL calculates fusion cross sections and the mean angular momenta of the CN under the influence of couplings between the relative motion and nuclear collective motions [17,18,67]. Statistical model [68–70] calculations have been carried out for $^{12}C + ^{182,184,186}W$ reac-

TABLE I. Measured evaporation residue cross-sections (σ_{ER}) for $^{12}C + ^{182,184,186}W$ reactions. The quoted errors include the statistical error plus the error in the estimation of transmission efficiency.

$^{12}C + ^{182}W$				$^{12}C + ^{184}W$				$^{12}C + ^{186}W$			
$E_{c.m.}$ (MeV)	E^* (MeV)	σ_{ER} (mb)	$\delta\sigma_{ER}$ (mb)	$E_{c.m.}$ (MeV)	E^* (MeV)	σ_{ER} (mb)	$\delta\sigma_{ER}$ (mb)	$E_{c.m.}$ (MeV)	E^* (MeV)	σ_{ER} (mb)	$\delta\sigma_{ER}$ (mb)
48.69	32.63	0.26	0.05	48.67	34.79	0.39	0.07	48.73	37.18	0.39	0.10
50.57	34.50	3.33	0.50	50.55	36.67	5.35	0.70	50.61	39.06	9.15	1.34
52.45	36.38	20	3	52.44	38.56	37	5	52.50	40.94	49	7
54.33	38.26	69	9	54.32	40.44	99	12	54.38	42.82	136	17
56.20	40.14	127	16	56.20	42.32	194	24	56.26	44.70	260	34
58.08	42.02	202	26	58.08	44.20	320	40	58.14	46.58	390	48
59.96	43.90	346	45	59.96	46.08	593	74	60.02	48.46	616	78
61.84	45.77	461	60	61.84	47.96	619	77	61.90	50.34	778	99
63.72	47.65	502	69	63.72	49.84	743	93	63.78	52.23	937	120
65.59	49.53	733	145	65.60	51.72	903	109	65.66	54.11	1267	156
67.47	51.41	1022	136	67.48	53.60	1018	129	67.54	55.99	1229	152
71.23	55.16	1007	174	71.24	57.36	1373	234	71.30	59.75	1639	290
74.98	58.92	1256	265	75.00	61.12	1575	298	75.06	63.51	1659	273
78.74	62.67	1252	231	78.75	64.87	1637	276	78.83	67.27	1925	332

tions and observed that the calculated fission cross sections are negligibly small in the measured energy region. At the highest measured laboratory energy, the fission is estimated to be 6%, 4%, and 2% for $^{12}C + ^{182}W$, $^{12}C + ^{184}W$, and $^{12}C + ^{186}W$ respectively. Fusion cross sections are the sum of ER cross sections (σ_{ER}) and fission cross section (σ_{fiss}). In these reactions, fission becomes significant only at very high excitation energies [53–56]. Considering this, in the measured energy range, we can equate capture cross sections (σ_{cap}), fusion cross sections, as well as σ_{ER} ($\sigma_{cap} \approx \sigma_{fus} \approx \sigma_{ER}$). Hence, the fusion cross sections calculated using CCFULL [17,18] directly compare with the measured ER (fusion) cross sections. For $^{12}C + ^{182}W$ reaction, the depth parameter of the Woods-Saxon potential $V_0 = 72$ MeV, the radius parameter $r_0 = 1.15$ fm, and the diffuseness parameter $a_0 = 0.70$ fm were used. These parameters were selected based on the nearest systems $^{16}O + ^{186}W$ [71] and $^{16,18}O + ^{181}Ta$ [11]. Considering the fact that the target nuclei differ in neutron number only, which will not have any bearing on the potential, we have used the same potential parameters $^{12}C + ^{182,184,186}W$ reactions. The measured fusion cross sections and CCFULL calculations are shown in Figs. 1(a)–1(c).

To explain the observed subbarrier cross sections, we have included the static deformation effects of the targets. For including the static deformation effects of deformed tungsten nuclei, we have taken into account their quadrupole (β_2) and hexadecapole (β_4) deformation parameters in the CCFULL calculations. We ignore the excitations in the projectile nucleus, ^{12}C, since their contribution is expected to be smaller than the effects of the target excitations. In Table II, we listed the β_2, β_4 deformation parameters and the excitation energies of the first 2^+ state in the ground state of the target nuclei. CC calculations for $^{12}C + ^{182,184,186}W$ reactions are represented by solid lines in Figs. 1(a)–1(c). For $^{12}C + ^{182}W$ reaction, CC calculations show good agreement with the measured fusion cross sections in the entire energy region. In the case of $^{12}C + ^{184,186}W$ reactions, CC calculations explain the experimental fusion cross sections at lower excitation energies. However, calculations show a deviation at higher excitation energies. If one uses a different potential, $V_0 = 105$ MeV, $r_0 = 1.15$ fm, and $a_0 = 0.71$ fm for the reaction $^{12}C + ^{184}W$ and $V_0 = 115$ MeV, $r_0 = 1.16$ fm, and $a_0 = 0.73$ fm for $^{12}C + ^{186}W$ reaction, CC calculations show good agreement with the measured fusion cross sections at higher excitation energies. However, with the use of these potential parameters, CC calculations overpredict the measured fusion cross sections at subbarrier energies. In Figs. 1(b) and 1(c), CC calculations with these modified potentials are also shown.

TABLE II. The deformation parameters and excitation energies [72,73] used for CCFULL calculation.

System	β_2	β_4	E_{2^+} (MeV)
^{182}W	0.251	−0.066	0.100
^{184}W	0.236	−0.093	0.111
^{186}W	0.226	−0.095	0.122

The $^{12}C + ^{186}W$ reaction is having a positive transfer Q value of 0.177 MeV for the $-2n$ transfer. All the other neutron transfer reactions have negative Q values. Without the inclusion of the effects of PQNT channel, the $^{12}C + ^{186}W$ reaction shows a reasonably good agreement with the CC calculations at sub-barrier energies, i.e., the PQNT have no effects on the observed subbarrier fusion cross sections of $^{12}C + ^{186}W$ reaction.

B. Statistical model calculations

The statistical model code HIVAP (Heavy-Ion VAPorisation statistical-evaporation model) [68–70] was used to investigate the de-excitation of the formed compound nuclei for $^{12}C + ^{182,184,186}W$ reactions. The HIVAP code makes use of the standard evaporation theory, which considers ER produc-

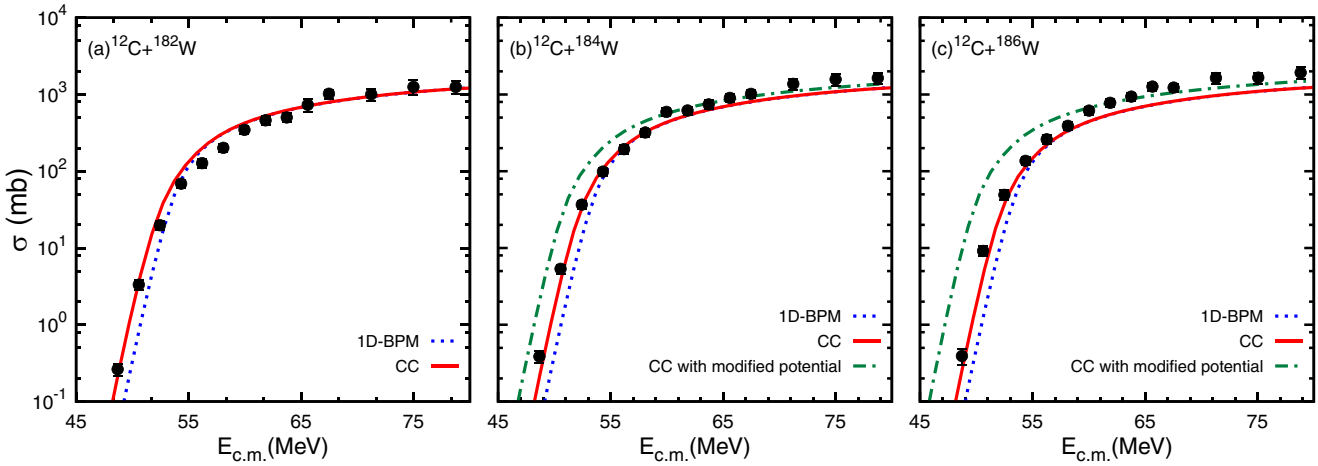

FIG. 1. Measured fusion excitation functions as a function of $E_{c.m.}$ for $^{12}C + ^{182,184,186}W$ reactions along with CC calculations in panels (a), (b) and (c) respectively. In panels (a)–(c), solid circles are the measured cross sections, dotted lines are 1D-BPM calculations with $V_0 = 72.0$ MeV, $r_0 = 1.15$ fm, and $a_0 = 0.70$ fm and solid lines represent CC calculations with these potential parameters. In panels (b) and (c), green dashed-dotted lines represent CC calculations with modified potential parameters, $V_0 = 105.0$ MeV, $r_0 = 1.15$ fm, and $a_0 = 0.71$ fm for $^{12}C + ^{184}W$ reaction and $V_0 = 115.0$ MeV, $r_0 = 1.16$ fm, and $a_0 = 0.71$ fm for $^{12}C + ^{186}W$ reaction.

tion processes as a two-step processes, i.e., (1) compound nucleus formation and (2) its entirely independent subsequent de-excitation. HIVAP code takes into account the competition between various decay channels, such as neutron, proton, and α-particle evaporation, γ-ray emissions, and fission. The fusion mechanism is assumed to occur whenever the projectile-target system overcomes the interaction potential barrier calculated from Bass's global nucleus-nucleus potential [74]. To estimate the cross sections at the subbarrier region, the WKB (Wentzel-Kramer-Brillouin) approximation is used. Coupled-channel effects are taken into account phenomenologically through the use of fluctuating barrier [75], which may be necessary at near and subbarrier energies. Level density parameters, fission barriers, and masses are the most sensitive parameters involved in the de-excitation processes. The Reisdorf and Schädel parameters [69] are the standard set of parameters used for this calculation in HIVAP code. Among this standard set of parameters, we varied the parameters of the nuclear potential to explain the measured ER cross sections for $^{12}C + ^{182,184,186}W$ reactions. In addition, we considered the effects of static deformation of the target on fusion probabilities below the threshold.

For mass-asymmetric systems, fission is significant only at energies well above the fusion barrier. At these high energies, fission has a significant influence on the production cross sections of ERs. The HIVAP calculation is primarily determined by the fission barrier scaling factor (k_f) of the liquid drop (LD) fission barrier ($B_f^{\rm LD}$) [76], which modify the fission barrier as

$$B_f(l) = k_f B_f^{\rm LD} + \delta W_{\rm g.s.} \qquad (2)$$

in which $\delta W_{\rm g.s.}$ is the ground-state shell correction. Level densities and nuclear masses are the main input parameters required to estimate the fission barrier. According to Reisdorf's macroscopic description [68,69], the nuclear level densities in fission and evaporation channels are provided by ratios of level densities $a_f/a_n \geqslant 1$, due to the different nuclear shapes at the saddle point (fission) and equilibrium state (particle emission).

Comparison of calculated and measured ER cross sections for $^{12}C + ^{182,184,186}W$ reactions are shown in Figs. 2(a), 2(b), and 2(c) respectively. These calculations reasonably reproduce the measured ER as well as fission cross sections [53–56]. In the inset figures, we show the fission cross sections available in the literature and their comparison with the calculations.

We have used $V_0 = 72$ MeV, $r_0 = 1.12$ fm, and $D = 0.62$ fm as potential parameters for all calculations using HIVAP. The effects of static deformations on fusion probability has been considered at subbarrier energies. Simultaneous analysis of fission and ER cross sections for $^{12}C + ^{182,184,186}W$ reactions allow us to obtain the value of fission barrier scaling parameter. The HIVAP calculations with $k_f = 0.96$ show good agreement with the measured fission cross sections for $^{12}C + ^{182,184,186}W$ reactions [53–56]. Furthermore, corresponding ER cross sections from HIVAP calculations agree fairly well with the measured ER excitation function. As mentioned in the introduction, Delagrange *et al.* [54] observed a large difference of the fission cross sections between ^{194}Hg and ^{198}Hg at $E^* = 82$ MeV formed by $^{12}C + ^{182,186}W$ reactions respectively ($\sigma_{\rm fiss} = 536 \pm 52$ mb for ^{194}Hg and $\sigma_{\rm fiss} = 166 \pm 68$ mb for ^{198}Hg). From the HIVAP calculations, at $E^* = 82$ MeV, we obtained $\sigma_{\rm fiss} = 521$ mb for ^{194}Hg CN and $\sigma_{\rm fiss} = 209$ mb for ^{198}Hg CN. This means our statistical model calculations with $k_f = 0.96$ for $^{12}C + ^{182,184,186}W$ reactions explains our measured ER as well as measured fission cross sections from literature [53–56]. When the ER and fission excitation functions are fairly in agreement with the calculations with the same parameter values of the nuclear potential and k_f (fission barrier scaling factor) across the whole range of excitation energy, the CN formation probability is usually assumed to be unity in the case of an asymmetric system [77]. The HIVAP calculations using same parameter values of the nuclear potential and k_f explain the measured ER excitation

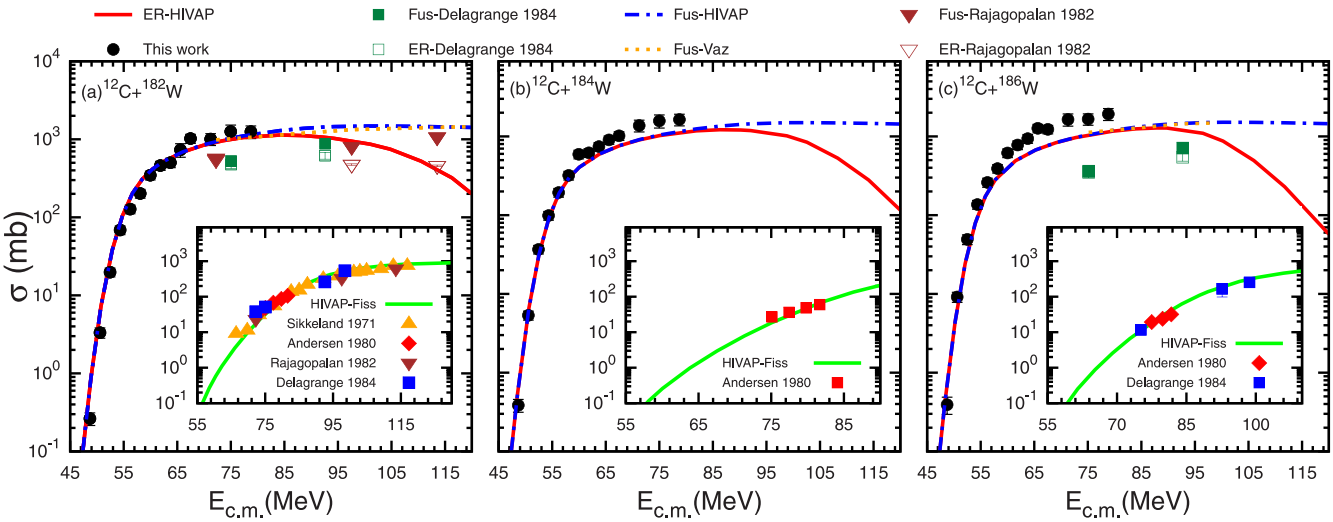

FIG. 2. Experimental ER, fission, and fusion excitation functions along with HIVAP calculations for $^{12}C + ^{182,184,186}W$ reactions shown in panels (a), (b) and (c) respectively. In the inset, the solid points represent measured fission cross sections [53–56] and solid lines represent the calculations using the code HIVAP.

function in the entire energy region for $^{12}C + ^{182,184,186}W$ reactions. This leads to the conclusion that the noncompound nuclear fission (NCNF) processes are not affecting the ER production of ^{12}C induced reactions forming $^{194,196,198}Hg$ CN. In the entire energy region, the measured ER and fission cross sections show reasonably good agreement with the statistical model calculations without including the dissipation or viscosity effects. This indicates the absence of dissipative effects in ER cross sections in the these reactions.

In Figs. 2(a), 2(c), and Table III, we compare present measurements for $^{12}C + ^{182,186}W$ reactions with the measurements performed by Rajagopalan *et al.* [53] and Delagrange *et al.* [54]. Also, in these figures, we have shown the present statistical model calculations along with the calculations based on systematics [53,54]. From these figures and from Table III, it is clear that the fusion cross sections measured by Rajagopalan *et al.* and Delagrange *et al.* are smaller by a factor of ≈2 compared to the present measurements for $^{12}C + ^{182}W$ reaction. Furthermore, in the case of $^{12}C + ^{186}W$ reaction, the fusion cross section measured by Delagrange *et al.* is smaller by a factor of ≈5 compared to the present measurements. However, our measured fusion cross sections show reasonably good agreement with the calculated fusion cross sections using various theoretical models and fusion systematics of Rajagopalan *et al.* and Delagrange *et al.* Considering these and the fact that our measurements show reasonably good agreement over the entire excitation energy range with statistical model calculations, we can say that the discrepancies observed by Rajagopalan *et al.* and Delagrange *et al.* may be attributed to the missing ER events in their measurements. It is important to mention that the discrepancies between fusion measurements and calculations based on various theoretical models and by fusion systematics of Rajagopalan *et al.* and Delagrange *et al.* are due to the absorption of low-energy evaporation residues in the target and/or various foils prior to entering the sensitive part of the detection system.

C. General remarks

Noncompound nuclear fission (NCNF) processes are usually not expected in reactions induced by ^{16}O and projectiles lighter than ^{16}O. However, a recent comprehensive study suggests that the NCNF may also play a role in ^{16}O-induced reactions [78]. In order to verify the entrance channel effects on the ER cross sections, ER measurements of additional systems that produce the $^{194–198}Hg$ CN and others close to these nuclei (A = 194–198) are considered for comparison

TABLE III. Comparison of present measurements for $^{12}C + ^{182,186}W$ reactions with Rajagopalan *et al.* [53] and Delagrange *et al.* [54].

	Present work	Rajagopalan [53]			Delagrange [54]		
E_{lab} (MeV)	σ_{ER} (mb)	σ_{ER} (mb)	σ_{fiss} (mb)	σ_{fus} (mb)	σ_{ER} (mb)	σ_{fiss} (mb)	σ_{fus} (mb)
			$^{12}C + ^{182}W$				
76	1007 ± 174						
77		545 ± 10	23 ± 8	568 ± 10		37.6 ± 3.5	
80	1256 ± 265				475 ± 50	51.2 ± 5.6	526 ± 50
			$^{12}C + ^{186}W$				
80	1659 ± 273				350 ± 50	11.60 ± 0.27	362±50

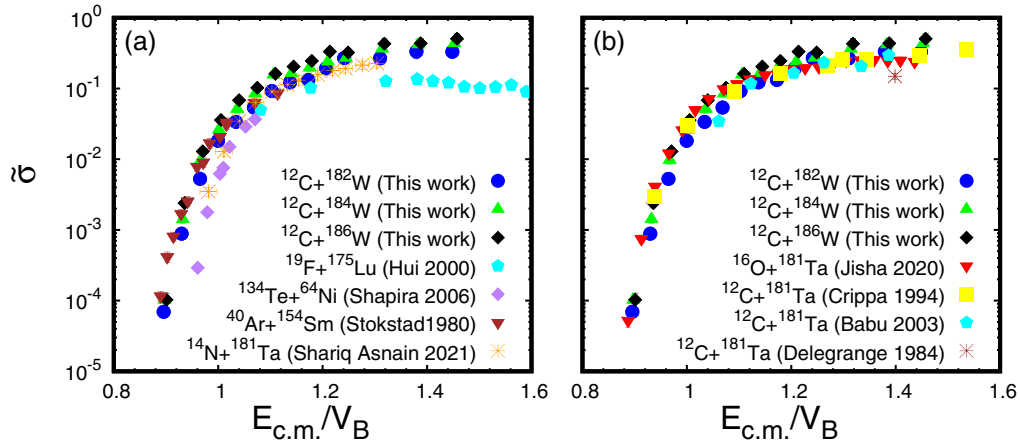

FIG. 3. Reduced cross sections as a function of $E_{c.m.}/V_B$ for reactions forming Hg CN and near to Hg. Here reduced cross sections ($\tilde{\sigma}$) is obtained by $\frac{\sigma_{ER}}{\pi R_B^2}$ and V_B is the Bass barrier.

with the present work. These are shown in Figs. 3(a) and 3(b), respectively.

To further explore the effects of the entrance channel, we compared the reduced cross-sections ($\tilde{\sigma} = \frac{\sigma_{ER}}{\pi R_B^2}$, where R_B is the Bass barrier radius) of ^{194,195,196,198}Hg CN formed by various projectile-target combinations, as shown in Fig. 3(a). If one compares $^{12}C + ^{182,184,186}W$ reactions, no noticeable effects on the subbarrier enhancement due to the addition of four neutrons (^{182}W to ^{186}W) is seen. In this figure, at higher excitation energies, $^{19}F + ^{175}Lu$ reaction shows a significant reduction in reduced cross sections, which has been attributed to the increase in the level density parameter ratio [59].

Figure 3(b) shows a comparison of reduced cross sections of ^{194,196,198}Hg CN with neighboring systems. A comparison of present measurements with neighboring systems does not show any significant effect of the entrance channel mass asymmetry over the entire energy range. For all reactions considered, the reduced cross sections are comparable at both below and above the barrier energy regions. When compared to the ERs measurements of the $^{12}C + ^{181}Ta$ reaction reported by Crippa *et al.* [79] and Babu *et al.* [80], the measurements by Delagrange *et al.* [54] show smaller cross sections at higher excitation energies.

Kozulin *et al.* [50] reported a large contribution of QF in the case of $^{68}Zn + ^{112}Sn$ reaction in comparison with $^{36}Ar + ^{144}Sm$ reaction, forming the same CN, ^{180}Hg. As mentioned in the introduction, the mean fissility parameter for the $^{68}Zn + ^{112}Sn$ reaction, $\chi_m = 0.695$, is just above the threshold value (0.68) for the presence of QF processes. When compared to the $^{36}Ar + ^{144}Sm$ reaction, the changes in the entrance channel properties are not as so drastic to cause such a large contribution of QF in the $^{68}Zn + ^{112}Sn$ reaction. The main difference between these two reactions is the entrance-channel mass asymmetry parameter (α), which drops from 0.60 for $^{36}Ar + ^{144}Sm$ to 0.24 for $^{68}Zn + ^{112}Sn$ reaction. Kozulin *et al.* [50] suggested that the influence of the entrance-channel mass asymmetry on QF processes is much stronger than previously assumed. To explore the dependence of fissility parameter and the entrance-channel mass asymmetry on the QF processes, we have studied even-even Hg CN from ^{180}Hg to ^{198}Hg. In addition to that two odd-even nuclei namely ^{185}Hg and ^{195}Hg also are considered.

We performed statistical model calculations for $^{40}Ar + ^{144-154}Sm$ [14], $^{48}Ti + ^{140,142}Ce$ [52], $^{19}F + ^{175}Lu$ [59], $^{16}O + ^{176,180}Hf$ [81], $^{90}Zr + ^{90-96}Zr$ [82–85], $^{86}Kr + ^{99-104}Ru$ [86], $^{124,130,134}Te + ^{58,64}Ni$ [87], and $^{14}N + ^{181}Ta$ [88] reactions. The results of the HIVAP calculations, as well as the measured cross sections (present measurements and measurements from the literature) for ^{180}Hg to ^{198}Hg CN are shown in Figs. 4(a)–4(l). From Figs. 4(a)–4(c), it is clear that the calculated ER cross sections for the reactions forming ^{180,182,184}Hg nuclei show slight deviation at below barrier energies in comparison with the measurements. This may be due to the approximations included in the coupling effects of the HIVAP calculations at these lower excitation energies.

We have performed statistical model calculations by varying fission barrier scaling factor k_f for majority of the asymmetric systems and able to find suitable values which can simultaneously reproduce the experimental fission and ER cross sections. In HIVAP calculations, the $k_f = 0.88$ for ^{180}Hg to ^{190}Hg CN and 0.96 for $^{192-198}$Hg CN were used. Also, the same k_f was used for neighboring reactions where no fission measurements are available. The static quadrupole moment for odd-even nuclei (^{181}Ta and ^{99}Ru) have been approximated by averaging the corresponding values in neighboring even-even nuclei. To explain the measured ER excitation functions of less asymmetric systems, we varied the CN formation probability (P_{CN}) from unity. P_{CN} is the probability that the dinuclear system crosses the inner fusion barrier and forms the CN. The deviation of P_{CN} from unity indicates the presence of QF or other NCNF processes. The entrance channel properties, $Z_P Z_T$, entrance-channel mass asymmetry (α), the mean fissility parameter (χ_m), effective fissility parameter (χ_{eff}), and CN formation probability (P_{CN}) for the reactions leading to the formation of $^{180-198}$Hg CN are listed in Table IV.

To explore the variation of P_{CN} with the entrance-channel mass asymmetry and the effective fissility parameter, we have plotted P_{CN} as a function of α and χ_{eff}, as shown in

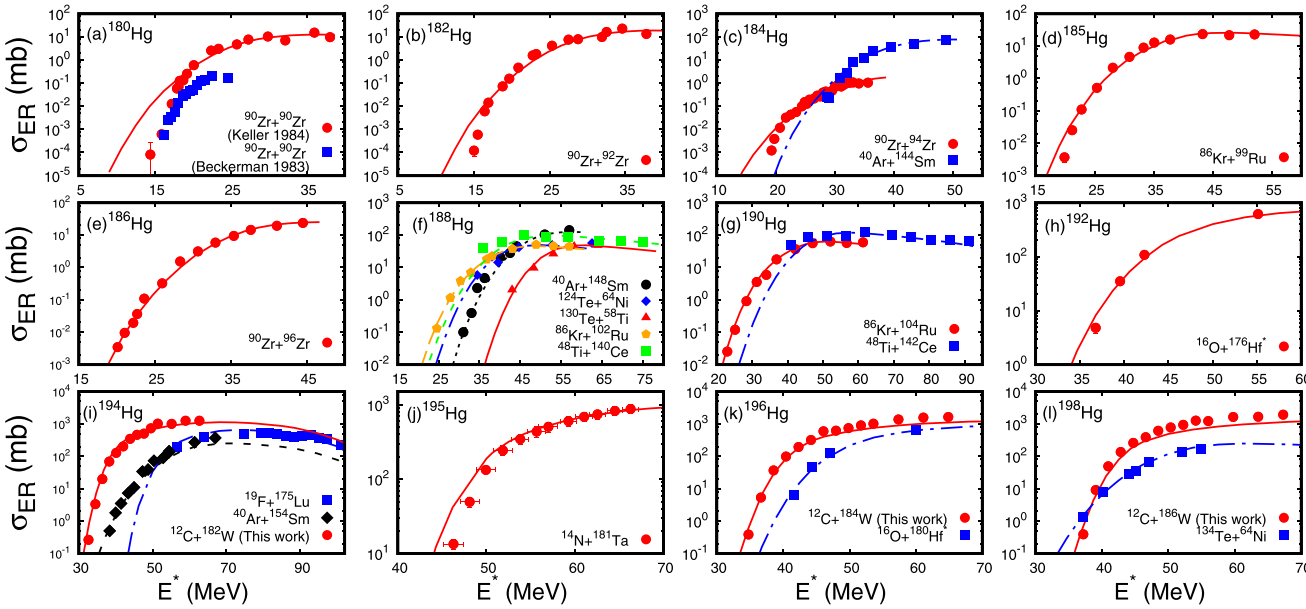

FIG. 4. Measured ER cross sections along with HIVAP calculations as a function of E^* for the reactions forming ^{180}Hg to ^{198}Hg CN (measured data includes the data available in literature and present ER measurements). Solid symbols are the experimental data and lines are the HIVAP calculations. In panels (h) and (k), in the case of $^{16}\mathrm{O} + ^{176,180}\mathrm{Hf}$ reactions, instead of σ_{ER} we have taken the measured σ_{fus} from literature [81].

Figs. 5(a) and 5(b) respectively. In these figures, the red points represent the $^{12}\mathrm{C} + ^{182,184,186}\mathrm{W}$ reactions. In Fig. 5(a), $^{124,130}\mathrm{Te} + ^{64,58}\mathrm{Ni}$ [87] reactions forming ^{188}Hg CN show a significant deviation of P_{CN} as a function of α compared to the other data sets. Similarly, in Fig. 5(b), $^{90}\mathrm{Zr} + ^{94}\mathrm{Zr}$ [84,85] shows a deviation of P_{CN} as a function of χ_{eff} compared to the other data sets. However, $^{124,130}\mathrm{Te} + ^{64,58}\mathrm{Ni}$ [87] reactions, which show large deviation in Fig. 5(a), do not show such large deviation of P_{CN} as a function of χ_{eff} in Fig. 5(b). Based on Figs. 5(a) and 5(b), we can conclude that reactions having $\chi_{\mathrm{eff}} \geqslant 0.64$ show presence of QF. If one considers entrance channel mass asymmetry, $\alpha \leqslant 0.2$ will show QF. Our

TABLE IV. The entrance channel properties and P_{CN} for the reactions leading to the formation of $^{180-198}$Hg.

Reaction	CN	$Z_P Z_T$	α	χ_m	χ_{eff}	P_{CN}	Ref.
$^{90}\mathrm{Zr} + ^{90}\mathrm{Zr}$	^{180}Hg	1600	0.0	0.714	0.714	0.35	[82–85]
$^{90}\mathrm{Zr} + ^{92}\mathrm{Zr}$	^{182}Hg	1600	0.011	0.710	0.710	0.48	[83]
$^{90}\mathrm{Zr} + ^{94}\mathrm{Zr}$	^{184}Hg	1600	0.022	0.705	0.705	0.05	[84,85]
$^{40}\mathrm{Ar} + ^{144}\mathrm{Sm}$	^{184}Hg	1116	0.565	0.613	0.583	1	[14]
$^{86}\mathrm{Kr} + ^{99}\mathrm{Ru}$	^{185}Hg	1584	0.070	0.699	0.697	0.50	[86]
$^{90}\mathrm{Zr} + ^{96}\mathrm{Zr}$	^{186}Hg	1600	0.032	0.701	0.701	0.48	[83]
$^{124}\mathrm{Te} + ^{64}\mathrm{Ni}$	^{188}Hg	1456	0.319	0.673	0.665	0.60	[87]
$^{130}\mathrm{Te} + ^{58}\mathrm{Ni}$	^{188}Hg	1456	0.383	0.684	0.680	0.70	[87]
$^{86}\mathrm{Kr} + ^{102}\mathrm{Ru}$	^{188}Hg	1584	0.085	0.693	0.692	0.60	[86]
$^{40}\mathrm{Ar} + ^{148}\mathrm{Sm}$	^{188}Hg	1116	0.574	0.609	0.580	1	[14]
$^{48}\mathrm{Ti} + ^{140}\mathrm{Ce}$	^{188}Hg	1276	0.489	0.644	0.627	1	[52]
$^{48}\mathrm{Ti} + ^{142}\mathrm{Ce}$	^{190}Hg	1276	0.495	0.641	0.622	1	[52]
$^{86}\mathrm{Kr} + ^{104}\mathrm{Ru}$	^{190}Hg	1584	0.095	0.690	0.689	0.65	[86]
$^{16}\mathrm{O} + ^{176}\mathrm{Hf}$	^{192}Hg	576	0.833	0.484	0.415	1	[81]
$^{12}\mathrm{C} + ^{182}\mathrm{W}$	^{194}Hg	444	0.876	0.440	0.358	1	This work
$^{19}\mathrm{F} + ^{175}\mathrm{Lu}$	^{194}Hg	639	0.804	0.495	0.431	1	[59]
$^{40}\mathrm{Ar} + ^{154}\mathrm{Sm}$	^{194}Hg	1116	0.588	0.639	0.577	1	[14]
$^{14}\mathrm{N} + ^{181}\mathrm{Ta}$	^{195}Hg	511	0.856	0.462	0.388	1	[88]
$^{12}\mathrm{C} + ^{184}\mathrm{W}$	^{196}Hg	444	0.878	0.441	0.358	1	This work
$^{16}\mathrm{O} + ^{180}\mathrm{Hf}$	^{196}Hg	576	0.837	0.481	0.415	1	[81]
$^{12}\mathrm{C} + ^{186}\mathrm{W}$	^{198}Hg	444	0.879	0.438	0.357	1	This work
$^{134}\mathrm{Te} + ^{64}\mathrm{Ni}$	^{198}Hg	1456	0.354	0.623	0.656	1	[87]

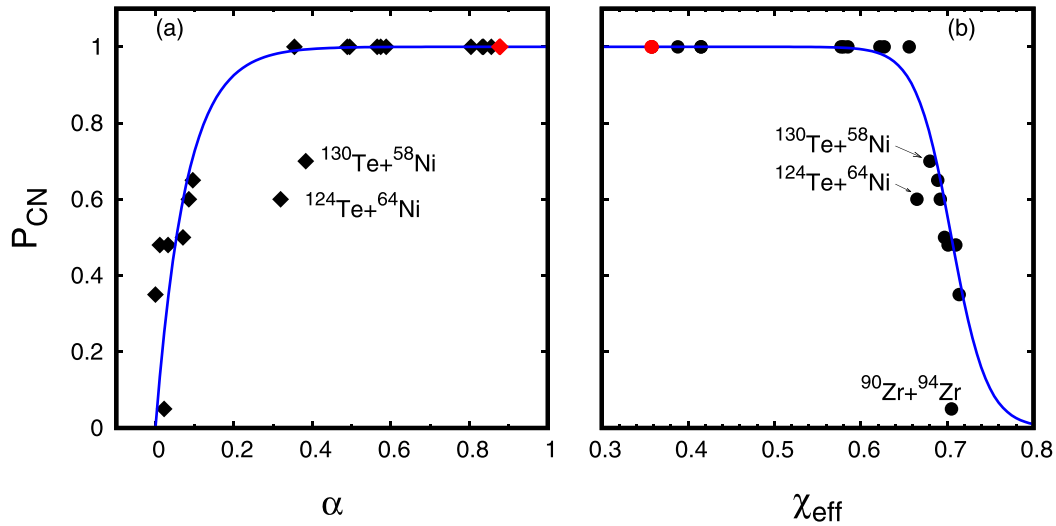

FIG. 5. Variation of P_{CN} as a function entrance channel mass asymmetry (α), and the effective fissility parameter (χ_{eff}). Red points are the data from this work and solid lines are a guide to the eye.

systematic analysis for $^{180–198}$Hg CN clearly shows the dependence of QF on α and the χ_{eff}. However, additional experiments with reactions leading to the formation of the Hg CN are needed to confirm these findings. In particular, the measurements of the reactions with mass asymmetry 0.1–0.3 and effective fissility parameter 0.63–0.70 are needed for better understanding.

V. SUMMARY AND CONCLUSION

Using a recoil mass spectrometer, we measured the ER excitation functions for $^{12}C + ^{182,184,186}W$ reactions leading to the formation of ^{194,196,198}Hg compound nuclei at energies 12% below to 45% above the Coulomb barrier. Coupled-channel calculations with the coupling of static deformation effects of target nuclei, using the selected potential parameters for $^{12}C + ^{182}W$ reaction, very well explains the measured fusion cross sections for $^{12}C + ^{182,184,186}W$ reactions in the subbarrier energy region. However, deviations from measured cross sections have been noticed at higher excitation energies for $^{12}C + ^{184,186}W$ reactions. Comparing $^{12}C + ^{182}W$, $^{12}C + ^{184}W$, and $^{12}C + ^{186}W$ reactions, we could not observe any noticeable effects on the subbarrier enhancement due to the addition of four neutrons.

The statistical model calculations with $P_{CN} = 1$ and $k_f = 0.96$ describe our measured ER as well as measured fission cross sections from literature [53–56]. From these results, we can conclude that the previously reported disagreement between measured and calculated fusion cross sections for $^{12}C + ^{182,186}W$ reactions [53,54] could be due to missing of ER events in their detection systems. We find no role of dissipative effects in the competition between fission and evaporation in $^{12}C + ^{182,184,186}W$ reactions in the measured energy region. Our systematic analysis for $^{180–198}$Hg CN shows the dependence of quasifission processes on entrance channel mass asymmetry and effective fissility. Additional experiments with reactions leading to the formation of the Hg CN with mass asymmetry 0.1–0.3 and effective fissility parameter 0.63–0.70 are needed to confirm these findings.

ACKNOWLEDGMENTS

We are grateful to the IUAC Pelletron group for providing an excellent beam with the required pulse width. We are thankful for the assistance provided by IUAC's target and data support laboratories. One of the authors (S.S.) acknowledges IUAC for financial assistance in the form of a fellowship.

[1] M. Dasgupta, D. J. Hinde, N. Rowley, and A. M. Stefanini, Annu. Rev. Nucl. Part. Sci. **48**, 401 (1998).
[2] B. B. Back, H. Esbensen, C. L. Jiang, and K. E. Rehm, Rev. Mod. Phys. **86**, 317 (2014).
[3] P. Kaur, M. Maiti, T. N. Nag, and S. Sodaye, Phys. Rev. C **105**, 014629 (2022).
[4] R. N. Sagaidak, M. L. Chelnokov, V. I. Chepigin, V. A. Gorshkov, O. N. Malyshev, A. G. Popeko, A. I. Svirikhin, and A. V. Yeremin, Phys. Rev. C **105**, 024604 (2022).
[5] F. Gollan, D. Abriola, A. Arazi, M. A. Cardona, E. de Barbará, J. de Jesús, D. Hojman, R. M. Id Betan, J. Lubian, A. J. Pacheco, B. Paes, D. Schneider, and H. O. Soler, Phys. Rev. C **104**, 024609 (2021).
[6] Vijay, R. P. Chahal, M. S. Gautam, S. Duhan, and H. Khatri, Phys. Rev. C **103**, 024607 (2021).
[7] N. Wang and W. Ye, Phys. Rev. C **103**, 024611 (2021).
[8] J. Gehlot, A. M. Vinodkumar, N. Madhavan, S. Nath, A. Jhingan, T. Varughese, T. Banerjee, A. Shamlath, P. V. Laveen,

M. Shareef, P. Jisha, P. S. Devi, G. N. Jyothi, M. M. Hosamani, I. Mazumdar, V. I. Chepigin, M. L. Chelnokov, A. V. Yeremin, A. K. Sinha, and B. R. S. Babu, Phys. Rev. C **99**, 034615 (2019).

[9] S. Nath, P. V. M. Rao, S. Pal, J. Gehlot, E. Prasad, G. Mohanto, S. Kalkal, J. Sadhukhan, P. D. Shidling, K. S. Golda, A. Jhingan, N. Madhavan, S. Muralithar, and A. K. Sinha, Phys. Rev. C **81**, 064601 (2010).

[10] Kavita, K. S. Golda, T. K. Ghosh, A. Jhingan, P. Sugathan, A. Chatterjee, B. R. Behera, A. Kumar, R. Kumar, N. Saneesh, M. Kumar, A. Yadav, C. Yadav, N. Kumar, A. Banerjee, A. Rani, S. K. Duggi, R. Dubey, K. Rani, S. Noor *et al.*, Phys. Rev. C **100**, 024626 (2019).

[11] P. Jisha, A. M. Vinodkumar, B. R. S. Babu, S. Nath, N. Madhavan, J. Gehlot, A. Jhingan, T. Banerjee, I. Mukul, R. Dubey, N. Saneesh, K. M. Varier, E. Prasad, A. Shamlath, P. V. Laveen, and M. Shareef, Phys. Rev. C **101**, 024611 (2020).

[12] J. R. Birkelund and J. R. Huizenga, Annu. Rev. Nucl. Part. Sci. **33**, 265 (1983).

[13] B. B. Back, D. J. Blumenthal, C. N. Davids, D. J. Henderson, R. Hermann, D. J. Hofman, C. L. Jiang, H. T. Penttilä, and A. H. Wuosmaa, Phys. Rev. C **60**, 044602 (1999).

[14] R. G. Stokstad, W. Reisdorf, K. D. Hildenbrand, J. V. Kratz, G. Wirth, R. Lucas, and J. Poitou, Z. Phys. A **295**, 269 (1980).

[15] A. Shrivastava, S. Kailas, A. Chatterjee, A. M. Samant, A. Navin, P. Singh, and B. S. Tomar, Phys. Rev. Lett. **82**, 699 (1999).

[16] C. Dasso, S. Landowne, and A. Winther, Nucl. Phys. A **405**, 381 (1983).

[17] K. Hagino, N. Rowley, and A. Kruppa, Comput. Phys. Commun. **123**, 143 (1999).

[18] K. Hagino and N. Takigawa, Prog. Theor. Phys. **128**, 1061 (2012).

[19] K. Hagino and J. M. Yao, EPJ Web Conf. **117**, 08003 (2016).

[20] K. Hagino, arXiv:2201.08061.

[21] M. Beckerman, M. Salomaa, A. Sperduto, H. Enge, J. Ball, A. DiRienzo, S. Gazes, Y. Chen, J. D. Molitoris, and Mao Naifeng, Phys. Rev. Lett. **45**, 1472 (1980).

[22] F. Scarlassara, S. Beghini, G. Montagnoli, G. Segato, D. Ackermann, L. Corradi, C. Lin, A. Stefanini, and L. Zheng, Nucl. Phys. A **672**, 99 (2000).

[23] Z. Kohley, J. F. Liang, D. Shapira, R. L. Varner, C. J. Gross, J. M. Allmond, A. L. Caraley, E. A. Coello, F. Favela, K. Lagergren, and P. E. Mueller, Phys. Rev. Lett. **107**, 202701 (2011).

[24] V. I. Zagrebaev, Phys. Rev. C **67**, 061601(R) (2003).

[25] L. T. Baby, V. Tripathi, D. O. Kataria, J. J. Das, P. Sugathan, N. Madhavan, A. K. Sinha, M. C. Radhakrishna, N. M. Badiger, N. G. Puttaswamy, A. M. Vinodkumar, and N. V. S. V. Prasad, Phys. Rev. C **56**, 1936 (1997).

[26] Khushboo, S. Mandal, S. Nath, N. Madhavan, J. Gehlot, A. Jhingan, N. Kumar, T. Banerjee, G. Kaur, K. Rojeeta Devi, A. Banerjee, Neelam, T. Varughese, D. Siwal, R. Garg, I. Mukul, M. Saxena, S. Verma, S. Kumar, B. R. Behera *et al.*, Phys. Rev. C **96**, 014614 (2017).

[27] G. L. Zhang, X. X. Liu, and C. J. Lin, Phys. Rev. C **89**, 054602 (2014).

[28] H. Timmers, D. Ackermann, S. Beghini, L. Corradi, J. H. He, G. Montagnoli, F. Scarlassara, A. Stefanini, and N. Rowley, Nucl. Phys. A **633**, 421 (1998).

[29] V. V. Sargsyan, G. G. Adamian, N. V. Antonenko, W. Scheid, and H. Q. Zhang, Phys. Rev. C **84**, 064614 (2011).

[30] A. M. Stefanini, G. Montagnoli, H. Esbensen, P. Čolović, L. Corradi, E. Fioretto, F. Galtarossa, A. Goasduff, J. Grebosz, F. Haas, M. Mazzocco, N. Soić, E. Strano, and S. Szilner, Phys. Rev. C **96**, 014603 (2017).

[31] A. N. Andreyev, J. Elseviers, M. Huyse, P. Van Duppen, S. Antalic, A. Barzakh, N. Bree, T. E. Cocolios, V. F. Comas, J. Diriken, D. Fedorov, V. Fedosseev, S. Franchoo, J. A. Heredia, O. Ivanov, U. Köster, B. A. Marsh, K. Nishio, R. D. Page, N. Patronis *et al.*, Phys. Rev. Lett. **105**, 252502 (2010).

[32] E. M. Kozulin, G. N. Knyazheva, I. M. Itkis, M. G. Itkis, Y. S. Mukhamejanov, A. A. Bogachev, K. V. Novikov, V. V. Kirakosyan, D. Kumar, T. Banerjee, M. Cheralu, M. Maiti, R. Prajapat, R. Kumar, G. Sarkar, W. H. Trzaska, A. N. Andreyev, I. M. Harca, A. Mitu, and E. Vardaci, Phys. Rev. C **105**, 014607 (2022).

[33] A. A. Bogachev, E. M. Kozulin, G. N. Knyazheva, I. M. Itkis, M. G. Itkis, K. V. Novikov, D. Kumar, T. Banerjee, I. N. Diatlov, M. Cheralu, V. V. Kirakosyan, Y. S. Mukhamejanov, A. N. Pan, I. V. Pchelintsev, R. S. Tikhomirov, I. V. Vorobiev, M. Maiti, R. Prajapat, R. Kumar, G. Sarkar *et al.*, Phys. Rev. C **104**, 024623 (2021).

[34] E. Prasad, D. J. Hinde, K. Ramachandran, E. Williams, M. Dasgupta, I. P. Carter, K. J. Cook, D. Y. Jeung, D. H. Luong, S. McNeil, C. S. Palshetkar, D. C. Rafferty, C. Simenel, A. Wakhle, J. Khuyagbaatar, C. E. Düllmann, B. Lommel, and B. Kindler, Phys. Rev. C **91**, 064605 (2015).

[35] K. Nishio, A. Andreyev, R. Chapman, X. Derkx, C. Düllmann, L. Ghys, F. Heßberger, K. Hirose, H. Ikezoe, J. Khuyagbaatar, B. Kindler, B. Lommel, H. Makii, I. Nishinaka, T. Ohtsuki, S. Pain, R. Sagaidak, I. Tsekhanovich, M. Venhart, Y. Wakabayashi *et al.*, Phys. Lett. B **748**, 89 (2015).

[36] S. Panebianco, J.-L. Sida, H. Goutte, J.-F. Lemaître, N. Dubray, and S. Hilaire, Phys. Rev. C **86**, 064601 (2012).

[37] H. Paşca, A. V. Andreev, G. G. Adamian, and N. V. Antonenko, Phys. Rev. C **101**, 064604 (2020).

[38] A. V. Andreev, G. G. Adamian, and N. V. Antonenko, Phys. Rev. C **86**, 044315 (2012).

[39] A. V. Andreev, G. G. Adamian, N. V. Antonenko, and A. N. Andreyev, Phys. Rev. C **88**, 047604 (2013).

[40] J. D. McDonnell, W. Nazarewicz, J. A. Sheikh, A. Staszczak, and M. Warda, Phys. Rev. C **90**, 021302(R) (2014).

[41] T. Ichikawa, A. Iwamoto, P. Möller, and A. J. Sierk, Phys. Rev. C **86**, 024610 (2012).

[42] P. Möller, J. Randrup, and A. J. Sierk, Phys. Rev. C **85**, 024306 (2012).

[43] C. Schmitt, A. Lemasson, K.-H. Schmidt, A. Jhingan, S. Biswas, Y. H. Kim, D. Ramos, A. N. Andreyev, D. Curien, M. Ciemala, E. Clément, O. Dorvaux, B. De Canditiis, F. Didierjean, G. Duchêne, J. Dudouet, J. Frankland, B. Jacquot, C. Raison, D. Ralet *et al.*, Phys. Rev. Lett. **126**, 132502 (2021).

[44] M. Warda, A. Staszczak, and W. Nazarewicz, Phys. Rev. C **86**, 024601 (2012).

[45] E. Prasad, D. Hinde, M. Dasgupta, D. Jeung, A. Berriman, B. Swinton-Bland, C. Simenel, E. Simpson, R. Bernard, E. Williams, K. Cook, D. Rafferty, C. Sengupta, J. Smith, K. Vo-Phuoc, and J. Walshe, Phys. Lett. B **811**, 135941 (2020).

[46] M. G. Itkis, N. A. Kondratev, S. I. Mulgin, V. N. Okolovich, A. Y. Rusanov, and G. N. Smirenkin, Sov. J. Nucl. Phys. **52**, 601 (1990).

[47] D. Kumar, E. M. Kozulin, M. Cheralu, G. N. Knyazheva, I. M. Itkis, M. G. Itkis, K. V. Novikov, A. A. Bogachev, N. I. Kozulina, I. N. Diatlov, I. V. Pchelintsev, I. V. Vorobiev, T. Banerjee, Y. S. Mukhamejanov, A. N. Pan, V. V. Saiko, P. P. Singh, R. N. Sahoo, A. N. Andreyev, D. M. Filipescu *et al.*, Bull. Russ. Acad. Sci. Phys. **84**, 1001 (2020).

[48] G. N. Knyazheva, E. M. Kozulin, R. N. Sagaidak, A. Y. Chizhov, M. G. Itkis, N. A. Kondratiev, V. M. Voskressensky, A. M. Stefanini, B. R. Behera, L. Corradi, E. Fioretto, A. Gadea, A. Latina, S. Szilner, M. Trotta, S. Beghini, G. Montagnoli, F. Scarlassara, F. Haas, N. Rowley, P. R. S. Gomes, A. Szanto de Toledo, and Phys. Rev. C **75**, 064602 (2007).

[49] T. Banerjee, D. J. Hinde, D. Y. Jeung, K. Banerjee, M. Dasgupta, A. C. Berriman, L. T. Bezzina, H. M. Albers, C. E. Düllmann, J. Khuyagbaatar, B. Kindler, B. Lommel, E. C. Simpson, C. Sengupta, B. M. A. Swinton-Bland, T. Tanaka, A. Yakushev, K. Eberhardt, C. Mokry, J. Runke *et al.*, Phys. Rev. C **102**, 024603 (2020).

[50] E. Kozulin, E. Vardaci, W. Trzaska, A. Bogachev, I. Itkis, A. Karpov, G. Knyazheva, and K. Novikov, Phys. Lett. B **819**, 136442 (2021).

[51] R. du Rietz, E. Williams, D. J. Hinde, M. Dasgupta, M. Evers, C. J. Lin, D. H. Luong, C. Simenel, and A. Wakhle, Phys. Rev. C **88**, 054618 (2013).

[52] D. P. Kaur, B. Behera, N. Madhavan, S. Nath, J. Gehlot, A. Kaur, Raghav, Gonika, R. Biswas, Subodh, Amit, A. Parihari, K. Rani, H. Arora, Shruti, and S. Pal, Nucl. Phys. A **1019**, 122384 (2022).

[53] M. Rajagopalan, D. Logan, J. W. Ball, M. Kaplan, H. Delagrange, M. F. Rivet, J. M. Alexander, L. C. Vaz, and M. S. Zisman, Phys. Rev. C **25**, 2417 (1982).

[54] H. Delagrange, A. Benachou, F. Hubert, Y. Llabador, B. Heusch, J. Coffin, P. Engelstein, P. Fintz, and G. Guillaume, Nucl. Phys. A **429**, 173 (1984).

[55] T. Sikkeland, J. E. Clarkson, N. H. Steiger-Shafrir, and V. E. Viola, Phys. Rev. C **3**, 329 (1971).

[56] J. U. Andersen, A. S. Jensen, E. Laegsgaard, K. O. Nielsen, J. S. Forster, I. V. Mitchell, D. Ward, and W. M. Gibson, *Proc. Conf. on Physics and Chemistry of Fission* (IAEA, Vienna, 1980), Vol. 1.

[57] J. M. Miller, D. Logan, G. L. Catchen, M. Rajagopalan, J. M. Alexander, M. Kaplan, J. W. Ball, M. S. Zisman, and L. Kowalski, Phys. Rev. Lett. **40**, 1074 (1978).

[58] J. M. Alexander, H. Delagrange, M. Rajagopalan, M. F. Rivet, and L. C. Vaz, Z. Phys. A **307**, 149 (1982).

[59] S. K. Hui, C. R. Bhuinya, A. K. Ganguly, N. Madhavan, J. J. Das, P. Sugathan, D. O. Kataria, S. Murlithar, L. T. Baby, V. Tripathi, A. Jhingan, A. K. Sinha, P. V. M. Rao, N. V. S. V. Prasad, A. M. Vinodkumar, R. Singh, M. Thoennessen, and G. Gervais, Phys. Rev. C **62**, 054604 (2000).

[60] A. Sinha, N. Madhavan, J. Das, P. Sugathan, D. Kataria, A. Patro, and G. Mehta, Nucl. Instrum. Methods Phys. Res., Sect. A **339**, 543 (1994).

[61] J. Gehlot, A. Jhingan, T. Varughese, S. Nath, and N. Madhavan, DAE Symp. Nucl. Phys. **65**, 782 (2021).

[62] B. P. Ajith Kumar, E. T. Subramaniam, and R. K. Bhowmik, http://www.iuac.res.in/NIAS.

[63] S. Nath, Comput. Phys. Commun. **180**, 2392 (2009).

[64] A. Gavron, Phys. Rev. C **21**, 230 (1980).

[65] http://lise.nscl.msu.edu/pace4.

[66] A. B. Balantekin and N. Takigawa, Rev. Mod. Phys. **70**, 77 (1998).

[67] http://www2.yukawa.kyoto-u.ac.jp/~kouichi.hagino/ccfull.html.

[68] W. Reisdorf, Z. Phys. A **300**, 227 (1981).

[69] W. Reisdorf and M. Schädel, Z. Phys. A **343**, 47 (1992).

[70] D. Vermeulen, H.-G. Clerc, C.-C. Sahm, K.-H. Schmidt, J. G. Keller, G. Münzenberg, and W. Reisdorf, Z. Phys. A **318**, 157 (1984).

[71] M. Z. Firihu, K. Hagino, and N. Takigawa, in *Fusion06: Reaction Mechanisms and Nuclear Structure at the Coulomb Barrier*, American Institute of Physics Conference Series Vol. 853, edited by L. Corradi, D. Ackermann, E. Fioretto, A. Gadea, F. Haas, G. Pollarolo, F. Scarlassara, S. Szilner, and M. Trotta (AIP, New York, 2006), pp. 309–314.

[72] S. Raman, C. Nestor, and P. Tikkanen, At. Data Nucl. Data Tables **78**, 1 (2001).

[73] P. Möller, A. Sierk, T. Ichikawa, and H. Sagawa, At. Data Nucl. Data Tables **109–110**, 1 (2016).

[74] R. Bass, Phys. Rev. Lett. **39**, 265 (1977).

[75] H. M. Devaraja, Y. K. Gambhir, M. Gupta, and G. Münzenberg, Phys. Rev. C **93**, 034621 (2016).

[76] A. J. Sierk, Phys. Rev. Lett. **55**, 582 (1985).

[77] R. N. Sagaidak and A. N. Andreyev, Phys. Rev. C **79**, 054613 (2009).

[78] T. Banerjee, S. Nath, and S. Pal, Phys. Rev. C **91**, 034619 (2015).

[79] M. Crippa, E. Gadioli, P. Vergani, G. Ciavola, C. Marchetta, and M. Bonardi, Z. Phys. A **350**, 121 (1994).

[80] K. S. Babu, R. Tripathi, K. Sudarshan, B. D. Shrivastava, A. Goswami, and B. S. Tomar, J. Phys. G: Nucl. Part. Phys. **29**, 1011 (2003).

[81] J. R. Leigh, J. J. M. Bokhorst, D. J. Hinde, and J. O. Newton, J. Phys. G: Nucl. Phys. **14**, L55 (1988).

[82] J. G. Keller, K.-H. Schmidt, H. Stelzer, W. Reisdorf, Y. K. Agarwal, F. P. Hessberger, G. Münzenberg, H.-G. Clerc, and C.-C. Sahm, Phys. Rev. C **29**, 1569 (1984).

[83] J. G. Keller, K. H. Schmidt, F. P. Hessberger, G. Münzenberg, W. Reisdorf, H. G. Clerc, and C. C. Sahm, Nucl. Phys. A **452**, 173 (1986).

[84] M. Beckerman, M. K. Salomaa, J. Wiggins, and R. Rohe, Phys. Rev. Lett. **50**, 471 (1983).

[85] M. Beckerman, J. Wiggins, H. Aljuwair, and M. K. Salomaa, Phys. Rev. C **29**, 1938 (1984).

[86] W. Reisdorf, F. P. Hessberger, K. D. Hildenbrand, S. Hofmann, G. Münzenberg, K.-H. Schmidt, W. F. W. Schneider, K. Sümmerer, G. Wirth, J. V. Kratz, K. Schutt, and C.-C. Sahm, Nucl. Phys. A **444**, 154 (1985).

[87] D. Shapira, F. Liang, C. Gross, R. Varner, J. Beene, A. Galindo-Uribarri, J. Campo, P. Hausladen, P. Mueller, D. Stracener, J. Kolata, and H. Amro, *Fusion06: Reaction Mechanisms and Nuclear Structure at the Coulomb Barrier*, edited by L. Corradi, D. Ackermann, E. Fioretto, A. Gadea, F. Haas, G. Pollarolo, F. Scarlassara, S. Szilner, and M. Trotta, American Institute of Physics Conference Series Vol. 853 (AIP, New York, 2006),pp. 402–407.

[88] M. S. Asnain, M. Shuaib, I. Majeed, M. K. Sharma, V. R. Sharma, A. Yadav, D. P. Singh, P. P. Singh, U. Gupta, R. N. Sahoo, A. Sood, M. Kaushik, S. Kumar, R. Kumar, B. P. Singh, and R. Prasad, Phys. Rev. C **104**, 034616 (2021).